2021-10-31

3D Printed Mechanically Modular Two-Degree-Of-Freedom Robotic Segment Utilizing Variable-Stiffness Actuators

Wilmot, A

10.1007/978-3-030-89177-0_24
Lecture Notes in Computer Science (including subseries Lecture Notes in Artificial Intelligence and Lecture Notes in Bioinformatics)
Springer International Publishing

3D printed mechanically modular two-degree-of-freedom robotic segment utilizing variable-stiffness actuators

Alfred Wilmot[1,2] & Ian S. Howard[2]
[1]University of Sheffield, Sheffield, S1 3JD, UK.
[2]SECAM, University of Plymouth, Plymouth, PL4 8AA UK.
aiawilmot1@sheffield.ac.uk, ian.howard@plymouth.ac.uk

Abstract: Here we describe the initial development of a 3D printed modular robotic segment that is driven by *variable stiffness actuators* (VSAs). The novelty of the presented work is the combination of cost-effective antagonist VSAs with mechanical modularity: this enables multiple segments to be used either as a stand-alone serpentine robot or as compliant joints that can easily be integrated into other robotic systems. The VSAs are comprised of antagonist DC motor pairs that separately actuate two orthogonal revolute joints via a viscoelastic tendon-based transmission system. The simplistic nature of the design also aims to minimize the effects of joint coupling. Joint-level control is performed on a microcontroller which transmits motor current and joint position information over USB to a computer. ROS packages, including those needed for *Gazebo* and *MoveIt!* were created to enable physics simulations and motion-planning of either a single isolated segment, multiple chained segments, or some combination of segments and other robotic devices. We present results of a preliminary physical prototype of one such robotic segment whose joint positions and co-contractions were manually controlled using a gamepad and subsequently visualized using the developed ROS packages. The dynamics of the VSA were analyzed and the joint-torque equations were derived as functions of tendon parameters, joint angles, and motor electrical characteristics.

Keywords: 3D-printing; variable-stiffness; passive-compliance; ROS.

1 Introduction

In recent years, there has been a growing research interest in the development of variable stiffness actuators, known as VSAs, that enable impedance control [1]. One of the major driving factors for developing such actuators is to address safety concerns regarding physical human-robot interaction (HRI). According to [2], there is a strong indication that VSAs enable safer and faster payload handling compared to purely rigid actuators. In this work, a prototype two-degree-of-freedom (2-DoF) mechanically modular VSA segment was developed to meet the HRI safety and performance criteria in a cost-effective manner by 3D-printing most components. Currently, the segment consists of embedded joint encoders and off-board current-sensing circuits for inferring motor load to control tendon stiffness. The sensor read-outs of a single segment were inspected using rqt-plot and were also used to control simulations in ROS. Although many compliant tendon-driven robots designs exist, few have a modular construction. One exception is the VSA-CubeBot,

which makes use of low-cost servo units, and whose performance characteristics were very thoroughly investigated and characterized [3]. Unlike the VSA-CubeBot, the design of the system we present here consists of internal wiring cavities that ensure cabling is routed away from pinching points, secondary tendon channels to address the risk of overloading segments at the base of multi-segment assemblies, and integration with ROS. The latter is key for further researching the controllability of multi-segment implementations in a timely manner as the ever-expanding ecosystem of ROS packages is rich with state-of-the-art open-source trajectory-planning libraries, along with other useful software stacks. Furthermore, the mechanical coupling implementation of the design we present here is inherently very mechanically stable, only requires a single bolt to chain two segments together, and is almost fully 3D printed. These and additional features which are important for both the practical and cost-effective application of such a system will be elaborated upon in the following sections.

2 Design considerations

Serpentine robots are effectively a compromise between continuum-style and conventional rigid robots, as they are characterized by many discrete joints connected via small rigid links. Given that the joints of serpentine robots can be clearly defined by a kinematic chain, modelling using Denavit-Hartenberg (DH) parameters is possible. This avoids the control challenges associated with continuum-style robotics, and the high degree of joint redundancy of multi-segment chains facilitates many inverse-kinematic solutions for a particular motion-plan, which is useful for obstacle avoidance in unstructured environments. However, as the number of segments increases so too does the torque experienced at the bottom-most segment. Hence, this latest prototype is most appropriate for use in neutrally buoyant environments, mounted overhead to a gantry, or as a robotic wrist. Improving the load-bearing capacity of multi-segment manipulators will be the subject of later studies as this will greatly broaden the potential applications of this system, such as for use as a cost-effective robotic arm mounted on a wheelchair. In order for a user to teleoperate the manipulator's end-effector to perform pick-place tasks, a closed-loop control model was required. This allowed a motion-planner to accept goal end-effector pose data from a gamepad or 6-DOF joystick, generate a set of actuator commands to achieve the planned trajectory, receive sensor feedback to determine whether the manipulator is following the planned trajectory, and finally either confirm that the goal position is reached or indicate a failure to execute the planned motion.

3 Segment design

As is illustrated in **Fig 2A**, the segment design adopted here consists of male & female mechanical coupling elements sandwiching two offset/orthogonal revolute joints and an actuator block above the female connector at the base of the segment. **Fig 1** demonstrates how the mechanical-modularity facilitated by these coupling elements enables the combination of multiple chain segments and the ease

with which other peripheral elements such as end-effectors can be incorporated. Each joint can be deflected from the centered upright position by 45 degrees in either direction, yielding a total *range-of-motion* (ROM) of 90 degrees per joint. Embedded into each joint is an I2C-capable Hall-effect rotary magnetic encoder that is oriented opposite a radially magnetized magnet. The top and bottom joint sections rotate relative to one-another, and given that the encoder is static relative to the bottom section while the magnet is static relative to the top, the magnet rotates in front of the encoder IC as the joint actuates. Viscoelastic tendons, originally developed for the GummiArm [4], were used to connect the actuators to their respective joints to impart both variable-stiffness and passive compliance characteristics onto the segment, thereby facilitating safe HRI capabilities on the hardware level. These tendons exhibit an approximately linear response for low co-contractions and a quadratic response for higher co-contractions. An antagonist pair is required as each motor can only pull the joint in a single direction and not push in the other. The benefit of this setup is that joint stiffness can be controlled by varying the tendon co-contraction. Given the reciprocal nature of stiffness and compliance, the joint can also be made more passively compliant by relaxing the antagonist pair. To modulate the stiffness in this manner, the viscoelastic element must behave like a non-linear spring, otherwise the stiffness is independent of tendon length. If the response is quadratic, then the joint stiffness is linearly dependent on co-contraction [5,6].

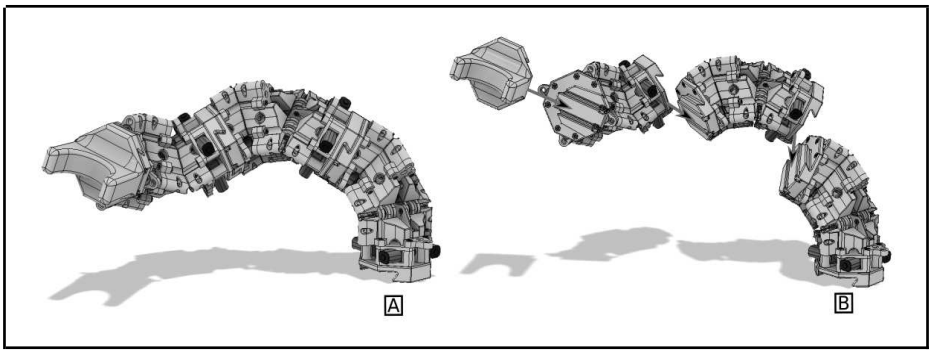

Fig. 1. Illustration of the segment's mechanical modularity. **A** Three segments are assembled together with a dummy end-effector at the distal-most end. **B** Illustrates how segments are fastened to each other using the mechanical coupling element.

4 Control electronics

The I2C communications protocol was chosen for an initial implementation due to its ease of use and extensive documentation. As can be seen in **Fig. 2G**, each joint is braced at two coupling points to mitigate axial torsion. Each coupling point consists of three bearing mount elements that are sandwiched together with an M3 bolt which is secured with a nut inserted into the head of the inside bearing mount. The M3 bolt straddles a steel axial bearing installed into the head of the central bearing mount. The magnet is placed into the head of the larger bearing mount facing the encoder. These bearing mounts are embedded into the joint plates and secured with M2 nuts and

bolts. The joint plates holding the bearing mounts are partially hollowed to internally accommodate cabling for the I2C BUS, thereby protecting electronics from direct impact with the environment or from being pinched between moving parts. The joints are symmetric, so they can be combined such that their axes of rotation are either parallel or orthogonal. The latter configuration was chosen since this results in a 3D workspace. As the system is tendon-driven from the base, the distal joint tendon length can be indirectly varied as the proximal joint moves through its range of motion. To mitigate the effects of joint coupling, the tendon-channel that intersects a joint's axis of rotation is brought as close to that axis as possible; this and all other design features are illustrated in **Fig. 2**.

5 Mechanical construction

Fused deposition modelling (FDM) is a 3D printing technique based on the layer-wise deposition of a thermoplastic filament from a heated nozzle. PLA was selected as the build material due to its affordability and ease of use. There is an inherent delamination strength associated with printed parts that is dependent on the material properties of the filament used and the surface area between printed layers. The orientation of the printed layers of a part relative to the forces that the part will experience when used had to be considered. The bearing mount elements were designed and printed in such a way as to maximize the joint's resistance to torque when under load and minimize the risk of delaminating printed layers. Furthermore, all printed parts were designed in such a way that few-to-no support structures were needed during manufacture, thereby reducing the post-processing overhead. The actuator block shown in **Fig. 2C** consists of an array of four DC motors where the tip of each motor shaft is braced by a bearing installed into the housing of an adjacent motor, thereby mitigating any moment experienced at the gearbox-shaft interface when the shaft is under load.

6 Position sensing and torque estimation

Joint angle and motor current-draw were monitored using PCBs fabricated by the authors. This enabled the variation of joint stiffness through controlling the tension applied to the tendons by the motors. Tendon tension is related to the torque exerted by the shaft of the motor, which in turn is related to the amount of current drawn.
Monitoring the current drawn by motors also means that safety-measures can be implemented to prevent them from being damaged. Modulating the applied voltage to control shaft velocity, thereby preventing overloading of the motor, will enhance the longevity of the system and enable joint torque control via tendon tension modulation. This also makes the system safer to use around people as the segment will be able to control the amount of force exerted as well as enforce low tendon tensions to ensure collisions result in minimal damage.

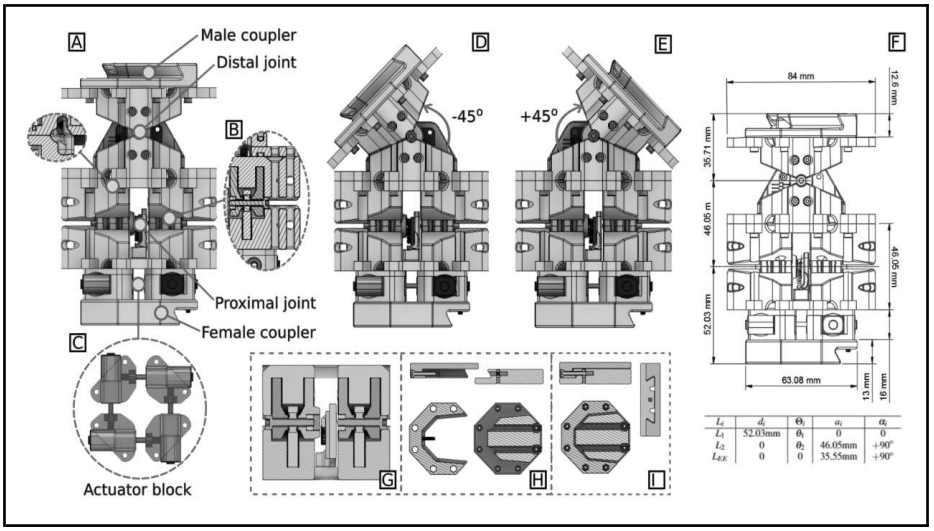

Fig. 2 Illustrations of segment design. **A** Internal channels in joint plates for routing electronics. **B** Proximal joint bearing mounts can be seen to the left. Of the two tendon channels towards the right, only the inner channel is used for connecting tendons to the actuator block associated with that segment. The outer channel is intended for a second set of tendons connected to powerful motors at the base of the segment-chain which pass through all segments and coupling to the distal-most segment. The viability of controlling a chain of segments in this manner is the subject of future work. **C** Layout of two antagonist pairs of brushed-DC motors forming the actuator block. **D**,**E** Illustrations of the 90-degree range of motion of the distal joint and mechanical hard-stops. **F** Table of DH parameters (bottom) and a schematic with the measurements that were used to calculate them (top). **G** Cross-sectional view of a rotary joint shows the position of the captive radially magnetized magnet (part of left axle) relative to the rotary magnetic encoder (located at the center of the joint). **H,I** Illustrations showing how the mechanical coupling element achieves a secure connection due to the tapered design using a single screw and captive nut.

7 Characterizing VSA dynamics

By considering the electrical characteristics of the DC motors used for the VSA, illustrated in **Fig**. **3A**, the generated torques can be derived as functions of *armature current* (i_a) its differential ($\dot{i}_a$), and shaft *angular velocity* (ω_m). This is shown in equation (1).

$$\tau_m = \frac{i_a}{\omega_m} \cdot (v_s - R \cdot i_a - L \cdot \dot{i}_a) \tag{1}$$

The joint openings α_r and α_l, referred to generally as α, relate to the *joint angle* (θ_j) according to equation (2).

$$\theta_j = \frac{\pi}{4} - \alpha_r = \alpha_l - \frac{\pi}{4} \tag{2}$$

The tendons exhibit a characteristic restorative force which we describe using the standard quadratic equation for simplicity, though in practice there is typically an initial region of linearity that is observed when the tendon is below a critical extension length, beyond which the response becomes quadratic. The constants of the quadratic equation shown in equation (3) are unique to each tendon and need to be determined through experimentation. Although the forces exerted on an individual tendon by either *joint torque* (τ_j) or *motor torque* (τ_m) are acting in opposite directions, the net *tendon displacement* (x) is positive. Hence, these forces can be considered as acting on a fixed tendon in the same direction, resulting in the expression shown in equation (3), where the torque lever arms are the joint-side lengths (a) and shaft radii (b), respectively.

$$\phi(x) = Ax^2 + Bx + C = \frac{\tau_m}{b} + \frac{\tau_j}{a} sin\left(\frac{\alpha}{2}\right) \tag{3}$$

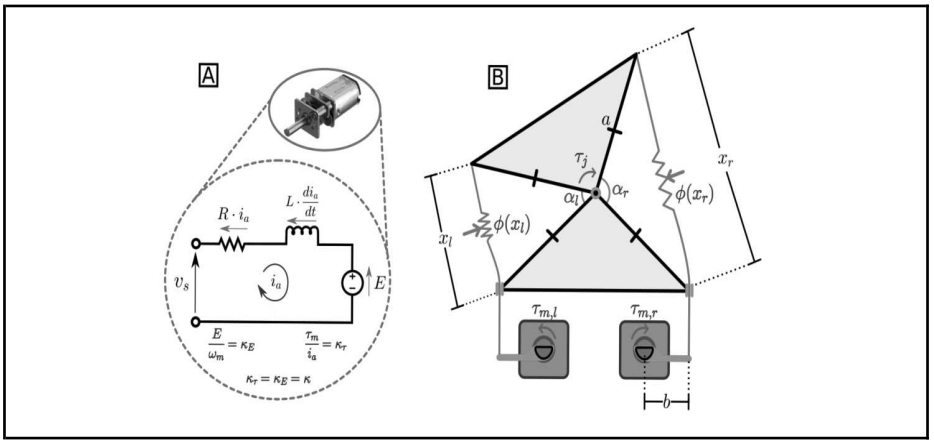

Fig. 3 Diagrams used to characterize the system dynamics. **A** Shows an equivalent electrical circuit of the DC motor used to drive the VSA. Definitions of the electrical constant (κ_E) and torque constant (κ_τ) are shown, and these are equivalent in the case of DC motors. This information is used to relate motor torque with its electrical characteristics. **B** Illustration of the geometric layout of a single VSA joint driven by an antagonist motor pair. Both tendons are assumed to exhibit identical responses for the same amount of deflection, governed by quadratic force functions ($\phi(x_l)$, $\phi(x_r)$), and as having lengths (x_l, x_r) that are functions of motor torque ($\tau_{m,l}$, $\tau_{m,r}$) and joint angle (θ_j). The effective shaft-radius (b) and joint side-lengths (a) affect the displacement characteristics for a particular motor shaft angle**.**

When the joint is static, the motor torque can be expressed purely in terms of the *tendon force function* ($\phi(x)$) of the tendon coupled to its shaft, as shown in equation (4).

$$\tau_m = \phi(x) \cdot b \tag{4}$$

Equation (5) shows that the displacement of an individual tendon is a function of both the joint angle and motor shaft position. This becomes apparent when we consider a co-contraction event: wherein the joint angle does not change, but the tendons are being elongated by their respective motors. The displacement due to the *joint position* (x_j) can be derived via the law of cosines, and that due to *movement of the motor shaft* (x_m) is the arc-length swept by the shaft as it rotates.

$$x = x_j + x_m = \left(a \cdot \sqrt{2} \cdot \sqrt{1 - \cos\left(\frac{\alpha}{2}\right)} \right) + (b \cdot \theta_m) \tag{5}$$

Given that we are treating the joint as being static when its stiffness is being modulated, the tendon displacement associated with this value can be treated as a constant, and so the derivative of the tendon displacement is purely that induced by the motor torque, resulting in equation (6).

$$\dot{x} = \dot{x}_m = b \cdot \omega_m \tag{6}$$

Therefore, when we combine equations (1), (3), (4), and (6), the result is the differential equation (7) that relates the tendon displacement due to the motor with the tendon parameters and the electrical characteristics of the motor.

$$\dot{x} = \frac{i_a \cdot (v_s - R \cdot i_a - L \cdot \dot{i}_a)}{Ax^2 + Bx + C} \tag{7}$$

In the case of a joint driven by an antagonist motor pair, as is illustrated in **Fig. 3B**, the torque experienced at the joint can be described as a function of the forces generated by these two opposing tendons, as shown in equation (8). The derivative of equation (8) with respect to *tendon displacements* (x_l, x_r) results in the joint stiffness, which needs to be controlled to achieve impedance control.

$$\tau_j = a \left(\frac{\phi(x_r)}{\sin\left(\frac{\alpha_r}{2}\right)} - \frac{\phi(x_l)}{\sin\left(\frac{\alpha_l}{2}\right)} \right) \tag{8}$$

In future work, these equations that govern the system dynamics will be used for the implementation for a state space controller. However, in this work, a facile implementation was set-up to manually demonstrate the impedance-controllable nature of the VSA using a gamepad.

8 Control and simulation using ROS

Various IK solving algorithms are available via the *MoveIt!* open-source motion-planning framework, which is a plugin for the *rviz* 3D visualization package available through the *Robot Operating System* (ROS). Motion-planning, preliminary qualitative simulations, and controlling the segment test-rig with a gamepad, were all performed using the ROS peer-to-peer nodal network of publishers and subscribers. To utilize ROS motion-planning packages, a *Universal Robotic Description File* (URDF) is needed. A URDF is essentially an xml-type file that describes how a robot's links and joints are arranged to form the resultant kinematic chain. URDFs treat a link's inertial, visual, and collision frames as separate entities. A Fusion360 plugin was used as a starting point for generating the URDF package from an assembly of the CAD model. Once finished, a ROS package is generated containing STLs representing each link, a URDF that references these STLs, and a launch-file that can be executed to visually debug the URDF in the *rviz* ROS package. When using *rviz*, a 3D representation of the system described by the URDF is shown in a GUI which includes track-bars for controlling what each virtual joint publishes to the *joint states* topic. **Fig. 4D** shows the corresponding system node-graph. Chapter 18 of Morgan Quigley's book, Programming Robots with ROS, was used as a guideline for setting up a ROS package that could utilize *MoveIt*! For motion planning, and simulations using the *Gazebo* physics engine.

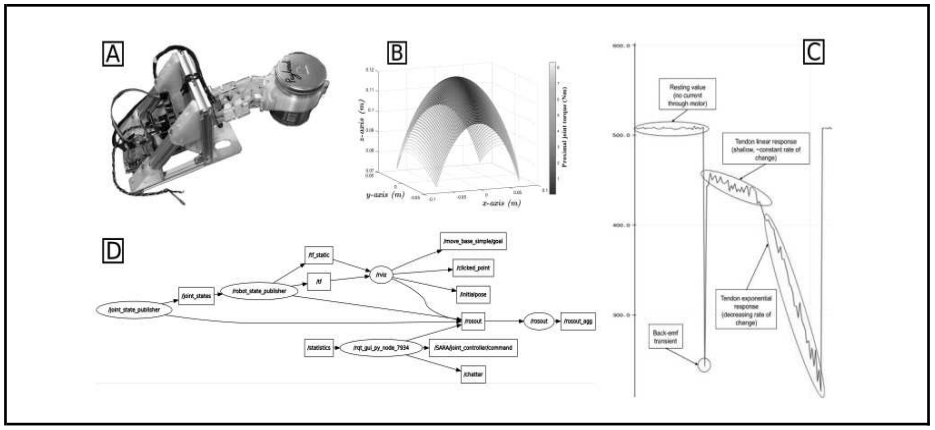

Fig. 4. Diagrams illustrating various aspects of the robot. **A** Testing platform for evaluating the performance characteristics of the developed segments. **B** Heat-map wherein each point indicates the reachable workspace of a single two-degree-of-freedom segment, and the color-coding indicates the corresponding theoretical torque experienced at the proximal joint of a single segment while a 10kg payload is connected to the distal joint at each point in the reachable workspace. **C** Annotated experimental current-measurements of a motor during a contraction event. There is a transient spike, an initial region of linearity as the tendon is being tensioned, then the quadratic response can be observed. **D** rqt node-graph showing how the GUI (the /joint_state_publisher node) controls the model in the rviz simulation (the /rviz node).

To perform experiments for evaluating the performance characteristics of the segment in a timely manner, a testing rig shown in **Fig. 4A** was constructed. Given that the tension of a particular tendon is inferred from the current drawn by its associated motor, the motor must be actively driving the joint for the tension to be modulated. For initial testing, tendon-tension modulation was controlled directly by the operator via a gamepad in order to experiment with various levels of co-contraction by manually modulating joint stiffness using the *rqt_plot* data-visualizer as a means of visually inferring the real-time joint stiffness and observe the system stability at different co-contraction levels.

9 MATLAB simulations and demo

To evaluate the effective workspace of the serpentine-segment, the kinematic chain was derived using conventional DH parameters, and the relevant measurements used to derive them are shown in **Fig. 2F**. To estimate the expected torque that a single segment would experience at its proximal joint when the end-effector is carrying a 10kg load, the inverse Jacobians of each possible joint configuration of the two joint setups were evaluated and multiplied with the force vector resulting from the 10kg load. The Forward-Kinematics of the segment for the joint-angle pair was evaluated in order to determine the (x,y,z) coordinates of the end-effector in the work-space. The end-effector coordinates were plotted on a 3D plot and the proximal joint torque associated with each end-effector position was encoded as a value for the heat-map shown in **Fig. 4B**.

In order to investigate the response characteristics of the segment under various loading conditions, the testing platform shown in **Fig. 5** was devised. This set-up enables the study of joint deflection angles under various loading conditions at particular tendon co-contractions. The degree to which the segment can be made to reliably follow a planned trajectory and recover from path deviations when perturbed can also be investigated, as well as the controllability of multi-segment systems.

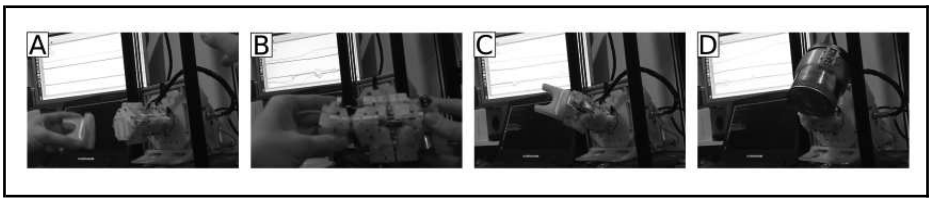

Fig.5 Demonstration of the 2-DOF VSA prototype. **A** The mechanically modular nature of the design can be demonstrated by placing an end-effector on a segment that is itself mounted to a testing platform. **B** The graphs in the background represent the joint angles (top) and the current-draw (bottom) of each motor. The resulting current-draw profile corresponds to the force generated by the segment as it attempts to maintain a particular joint configuration when deflected by an external force. This enables the system to exert either a known amount of force or comply (relax the tendons) as needed. **C,D** Actuation of the segment while an end-effector is mounted with either a stable mass (C), or an unstable mass (D). Link to video of demo.

10 Discussion

A modular 2-DOF actuator was developed, and some preliminary evaluations were made using a testing platform. A simple closed-loop controller demo with teleoperation was devised, ROS packages were created for motion-planning and physics simulations, and further analysis was also performed using MATLAB. Overall, this project involved the design and development of mechanical, electronic, and software components. Future developments will explore the scalability of the system and investigate embedding all the electronics used to control the segment into the segment body itself, such that the mechanical coupling of multiple segments places them on a common communications bus. The joint-torque equations presented were derived as functions of motor current and joint positions and are the first steps towards realizing simultaneous closed-loop control of the segment's joint positions and exerted torques (impedance control).

11 Acknowledgments

The authors would like to thank the University of Plymouth for supporting this work, *Access Robotics Ltd* for funding this research with a grant from the *European Regional Development Fund* (ERDF), and Dr. Federico Belmonte Klein for developing the Fusion360 URDF-generator plugin while also providing guidance in its use.

References

1. G. Grioli, S. Wolf, M. Garabini, M. Catalano, E. Burdet, D. Caldwell,R. Carloni, W. Friedl, M. Grebenstein, M. Laffranchi, D. Lefeber,S. Stramigioli, N. Tsagarakis, M. van Damme, B. Vanderborght,A. Albu-Schaeffer, and A. Bicchi, "Variable stiffness actuators: The user's point of view,"The International Journal of RoboticsResearch, vol. 34, no. 6, pp. 727–743, 2015. [Online]. Available:https://doi.org/10.1177/0278364914566515
2. A. Bicchi and G. Tonietti, "Fast and "soft-arm" tactics [robot arm design]," IEEE Robotics Automation Magazine, vol. 11, no. 2, pp. 22–33, June 2004.
3. Catalano, M. G., Grioli, G., Garabini, M., Bonomo, F., Mancini, M., Tsagarakis, N., & Bicchi, A. (2011, May). VSA-CubeBot: A modular variable stiffness platform for multiple degrees of freedom robots. In *2011 IEEE international conference on robotics and automation* (pp. 5090-5095). IEEE.
4. M. F. Stoelen, F. Bonsignorio, and A. Cangelosi, "Co-exploring actuator antagonism and bio-inspired control in a printable robot arm," in International Conference on Simulation of Adaptive Behavior. Springer,2016, pp. 244–255.
5. R. v. Ham, T. Sugar, B. Vanderborght, K. Hollander, and D. Lefeber, "Compliant actuator designs,"IEEE Robotics & Automation Magazine,vol. 3, no. 16, pp. 81–94, 2009.
6. S. A. Migliore, E. A. Brown, and S. P. DeWeerth, "Biologically inspired joint stiffness control," in Proceedings of the 2005 IEEE international conference on robotics and automation. IEEE, 2005, pp. 4508–4513.